JPE 17-3-4

https://doi.org/10.6113/JPE.2017.17.3.610
ISSN(Print): 1598-2092 / ISSN(Online): 2093-4718

Modified Finite Control Set-Model Predictive Controller (MFCS-MPC) for quasi Z-Source Inverters based on a Current Observer

Abualkasim Bakeer*, Mohamed A. Ismeil*, and Mohamed Orabi†

*,†Aswan Power Electronics Applications Research Center (APEARC), Aswan University, Aswan, Egypt

Abstract

The Finite Control Set-Model Predictive Controller (FCS-MPC) for quasi Z-Source Inverters (qZSIs) is designed to reduce the number of sensors by proposing a current observer for the inductor current. Unlike the traditional FCS-MPC algorithm, the proposed model removes the inductor current sensor and observes the inductor current value based on the deposited prior optimized state as well as the capacitor voltage during this state. The proposed observer has been validated versus a typical MPC. Then, a comparative study between the proposed Modified Finite Control Set-Model Predictive Controller (MFCS-MPC) and a linear PID controller is provided under the same operating conditions. This study demonstrates that the dynamic response of the control objectives by MFCS-MPC is faster than that of the PID. On the other hand, the PID controller has a lower Total Harmonic Distortion (THD) when compared to the MFCS-MPC at the same average switching. Experimental results validate both methods using a DSP F28335.

Key words: Current Observer, Finite Control Set-Model Predictive Control (FCS-MPC), quasi Z-Source Inverter (qZSI), Total Harmonics Distortion (THD)

I. INTRODUCTION

Short-circuits across the supply and the bucking-feature are the main drawbacks of the traditional Voltage Source Inverter (VSI). A new topology, referred to as a Z-Source Inverter (ZSI), that overcomes the obstacles of VSIs has been introduced in [1]. The ZSI has both bucking and boosting functionality within a single-stage without using more switching devices. Through the shoot-through criteria, the reliability of the inverter is improved. Short-circuits become allowable and the input voltage can be boosted up to the anticipated level. This new family of inverters has become a fertile area for researchers, and it encourages them to push their features forward. The quasi ZSI (qZSI) topology has been developed as an improvement of the original ZSI. It has extra features when compared to the classical ZSI [2], [3], such as a continuous drawn current from the source, and a low voltage stress on the capacitor (C_2).

From a control point of view, the ZSI family has two independent control freedoms which are: the shoot-through duty cycle (D) and the modulation index (M). These control signals can be used to control both the DC side (DC link voltage or capacitor voltage) and the AC side (output current or output voltage). For controlling the DC side, the DC link voltage of the boosting stage is the main control goal in the traditional two-stage inverter as it has a DC profile. On the other hand, in the ZSI family, the DC link voltage has a pulsating shape and there are two control approaches which are: direct and indirect ways [4]. The direct way utilizes hardware circuits to average the pulsated signal into a DC voltage [5]. Although the direct way has an improved the transient response and the disturbance rejection, it increases the cost and complexity of the control system. With the indirect way, both the input voltage and the capacitor (C_1) voltage are sensed to estimate the peak value of the DC link voltage [6]. Then the capacitor voltage is controlled to keep the average voltage of the DC link constant [7]. After that, the unified control technique was proposed to address the limitation between (D) and (M) with one degree of freedom ($D\ or\ M$). The output AC voltage can be regulated by the modulation index, whereas the capacitor voltage is kept variable [8].

Manuscript received Jun. 6, 2016; accepted Jan. 26, 2017
Recommended for publication by Associate Editor Honnyong Cha.
†Corresponding Author: orabi@ieee.org
Tel: +20-1001885361, Fax: +20-466-1406, Aswan University
*Dept. of Electrical Eng. Faculty of Eng., Aswan University, Egypt

Model Predictive Control (MPC) has become more predominant in power converter control. It promises some significant advantages for the converter control. For example, MPC can easily handle multiple variables with their boundaries and nonlinearities within a single control law as well as its concept is simple and intuitive [9]-[12]. Finite Control Set-MPC (FCS-MPC) chooses the optimized state for the converter and applies it directly to the converter switches. The FCS-MPC notion depends mainly on predicting the behavior of the controlled variables in future by using their discrete model. The development of rapid and powerful microprocessors makes the application of FCS-MPC in power electronics more attractive [13]. The control action in the future is achieved by a cost or objective function. The cost function is composed by the absolute error among the prediction values of the control objectives and their reference points. Each term in the cost function has a weighting factor that reflects the importance of the control variable in selecting the future actuation of switches. To date, there is no mathematical rule for specifying the value of the weighting factors. However, some guidelines were presented to reduce the uncertainty of the adjusting process in [14].

Recently, FCS-MPC has been integrated in the ZSI family to control both the DC side (capacitor voltage control with the requirement of sensing the inductor current) and the AC side (current control). Recent papers have been published in this direction [15]-[23]. In [15], the authors demonstrated a discrete model for the inductor current and capacitor voltage. The overall system was verified based solely on the simulation results. In [16], a FCS-MPC was applied to a Z-Source with a neutral point clamped inverter connected to the grid. In addition, only simulation results for the presented technique were given. The authors of [17] introduced a FCS-MPC for Maximum Power Point Tracking (MPPT) with a ZSI. However, only simulation results were provided in this case as well. After that, a FCS-MPC was introduced for a qZSI [18]-[22]. In [18], a model of a FCS-MPC with a qZSI was derived. For the first time, a real time implementation was presented along with simulation results. In [19], a qZSI was connected to the utility grid and the control was achieved by a FCS-MPC. In [20], a real time implementation was introduced based on dSPACE 1103 for a three-phase qZSI grid connected system. In [21], a parallel algorithm of a FCS-MPC was presented using a high speed FPGA board and SiC switched devices (rapid switching with low switching losses). Accordingly, the size and ripple of the qZSI were effectively reduced by increasing the switching frequency of the system. In [22], a FCS-MPC was applied to a switched-inductor qZSI where a discrete model of the converter was derived and the proposed control was experimentally validated.

The calculation time of any algorithm of a MPC is an important factor. Therefore, the authors proposed a modified algorithm that reduces the number of calculations in [23]. The algorithm saves the computational power of digital processor at executing the whole control system. This significant feature is obtained by removing the inductor current from the main cost function and keeping it as a sub-cost function to select either the shoot-through case or the non-shoot-through case. Choosing the shoot-through case from the start without passing through the loop reduces the number of calculations.

However, the common feature of all these references is the necessity to use higher number of sensors, five sensors. These five sensors include three-current sensors for output AC currents, a current sensor for the inductor current, and a voltage sensor for the capacitor voltage. It worth to mention that a larger number of sensors increases the solution footprint and cost. The authors have proposed a simplified model using only three sensors and an algorithm was presented with only simulation results in [24]. Therefore, in this paper, an experimental validation for the inductor current observation is provided. The measured inductor current is replaced by the proposed observation methodology to predict the capacitor voltage. The methodology is derived according to an acknowledgment of the optimized switching state at the $(k-1)$ instant and the capacitor voltage during this state. In addition, an accurate discrete model of the inductor current is used to obtain the value of the inductor current at the (k) instant.

Reducing the number of circuit sensors in MFCS-MPC may affect the features of the control performance. Therefore, it should be compared to the conventional FCS- MPC in addition to the traditional PWM linear controller. A PID controller is used as the reference classic controller. It worth noting that some comparisons have been introduced in the literature. Unfortunately, all the previous comparisons done with a PID for a quasi Z-Source Inverter have ignored or missed some of the parameters which make the comparisons unfair or inaccurate. This is the main purpose for adding the comparison part in this paper. In [21] and [25], a parallel algorithm for the FCS-MPC of a qZSI versus the traditional PID controller was assessed. The conventional MPC described in [21] is the used one in the comparison. The main issue in this comparison is that the two controllers did not use the same switching frequency. Moreover, the capacitor reference voltages did not have the same value with the two schemes. Therefore, the provided comparison in this paper is adjusted to have the same power circuit, averaging switching frequency, reference values, and sampling period.

II. Description of the Modified Finite Control Set-Model Predictive Control Based Current Observer

The developed algorithm for the MFCS-MPC starts by measuring the three-phase currents and capacitor voltage $v_{C_1}(k)$. Here, for the symmetry and balancing of the three-phases RL load, only current of two phases are sensed

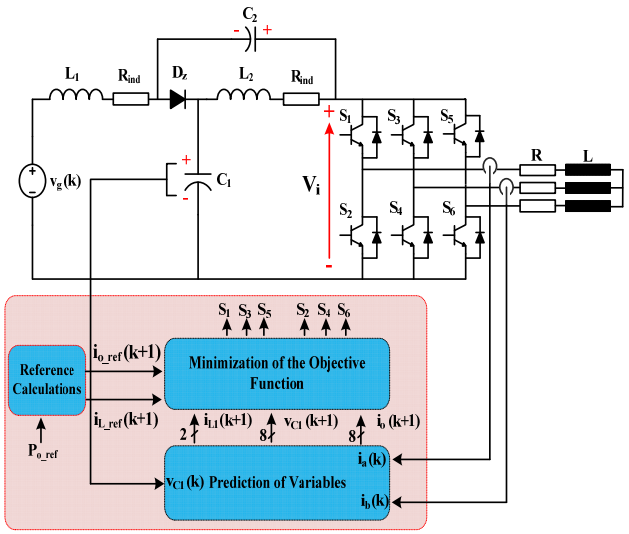

Fig. 1. MFCS-MPC for qZSI topology.

and the third is deduced using KCL [26]. However, under the asymmetry load condition, three-current sensors are required to measure the load currents. The whole MFCS-MPC system for a qZSI is shown in Fig. 1.

A. Model of the Controlled Variables

1) Load Current: All the three-phase quantities are converted into the (α, β) frames based on a classical Clarke transformation [27]. The space vector of the output voltage across the load $V_x(k+1)$ can be defined as:

$$V_x(k+1) = \frac{2.V_{dc}}{3}\left(S_a + a.S_b + a^2.S_c\right) \quad (1)$$

where, $x = [0:7]$, V_{dc} is the peak value for the DC link voltage which equals $(2.v_{C_1}(k) - v_g(k))$, $a = e^{j(2\pi/3)}$, and S_a, S_b and S_c are the switching states (either 0 or 1) for phase a, b and c, respectively.

The relation between the load current $i_o(k)$ at (k) instant, the future load current in the next sampling time $i_o(k+1)$, and the space vector of the output load voltage $V_x(k+1)$ can be derived as:

$$V_x(k+1) = R.i_o(k) + L.\frac{di_o(k)}{dt} \quad (2)$$

where, T_s, R and L are the sampling period, the resistance, and inductance of RL load, respectively.

The above derivative term for the load current can be approximated according to Euler method. Thus, the future value of the load current by which the behavior of the controlled load current can be predicted, is given by:

$$i_o(k+1) = \frac{T_s.V_x(k+1) + L.i_o(k)}{L + R.T_s} \quad (3)$$

After defining the discrete model for load current, its peak reference value, i_{o_ref}, should be set according to the reference output power, P_{o_ref}. This peak value is multiplied by three-phase sine waves shifted by 120 degree to have a sinusoidal shape and to be converted into (α, β) vectors. The prediction value of the output current during the next state $(k+1)$ is calculated in all the possible switching states of the inverter (there are eight states).

2) Inductor Current Observer and Capacitor Voltage: To complete the FCS-MPC algorithm for a qZSI, the model of capacitor voltage and inductor current should be stated. For the sake of simplicity, the capacitance of two capacitors are assumed equivalent as well as the inductance of two inductors. Moreover, the system is assumed operating in the Continuous Conduction Mode (CCM). The Equivalent Series Resistance (ESR) of the two capacitors is ignored to simplify the capacitor voltage model. It is known that there are two cases for the operation of a qZSI. These cases are non-shoot through and shoot-through.

a) Non Shoot-through Case: This can be signified as the active states; where there is an explicit relationship between the load and DC input source as shown in Fig. 2(a). The inductor (L_1) voltage and the capacitor (C_1) current during this case can be expressed as:

$$L_1.\frac{di_{L_1}(k)}{dt} = v_{C_1}(k) - v_g(k) + R_{ind}.i_{L_1}(k) \quad (4)$$

$$C_1.\frac{dv_{C_1}(k)}{dt} = i_{L_1}(k) - i_{inv}(k) \quad (5)$$

where, L_1 and C_1 are the inductance and capacitance of LC network in qZSI circuit, R_{ind} is the stray resistance of the inductor, $v_g(k)$ is the input DC source which is constant in the proposed algorithm, $i_{inv}(k)$ is the inverter output current that can be formulated as a function of the switching states as $i_{inv}(k) = i_a(k)(S_a - S_c) + i_b(k)(S_b - S_c)$, $v_{C_1}(k)$ is the capacitor voltage, and $i_a(k), i_b(k)$ and $i_{L_1}(k)$ are the currents of phase a, phase b and inductor (L_1) at the (k) instant.

Through simplifying the derivative term, the future inductor current, $i_{L_1}(k+1)$, and the future capacitor voltage, $v_{C_1}(k+1)$, during this case can be given as:

$$i_{L_1}(k+1) = \frac{T_s.(v_g(k) - v_{C_1}(k)) + L_1.i_{L_1}(k)}{L_1 + R_{ind}.T_s} \quad (6)$$

$$v_{C_1}(k+1) = v_{C_1}(k) + \frac{T_s}{C_1}(i_{L_1}(k+1) - i_{inv}(k+1)) \quad (7)$$

b) Shoot-through Case: When the shoot-through state is created, the two capacitors discharge their energy into the two inductors, and the diode turns off as shown in Fig. 2(b). The inductor voltage and capacitor current at this case can be expressed as:

$$L_1.\frac{di_{L_1}(k)}{dt} = v_{C_1}(k) + R_{ind}.i_{L_1}(k) \quad (8)$$

$$C_1.\frac{dv_{C_1}(k)}{dt} = -i_{L_1}(k) \quad (9)$$

The future inductor current and capacitor voltage in the shoot-through state can be determined by shifting the discrete-time equations (8) and (9) one step ahead as:

$$i_{L_1}(k+1) = \frac{T_s.v_{C_1}(k) + L_1.i_{L_1}(k)}{L_1 + R_{ind}.T_s} \quad (10)$$

$$v_{C_1}(k+1) = v_{C_1}(k) - \frac{T_s}{C_1}i_{L_1}(k+1) \quad (11)$$

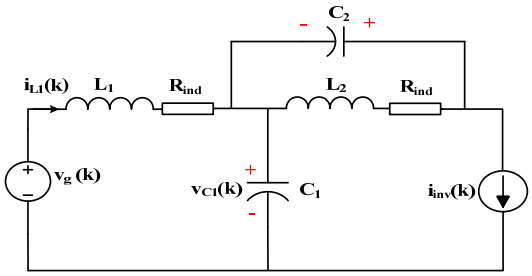

(a) Non shoot-through case.

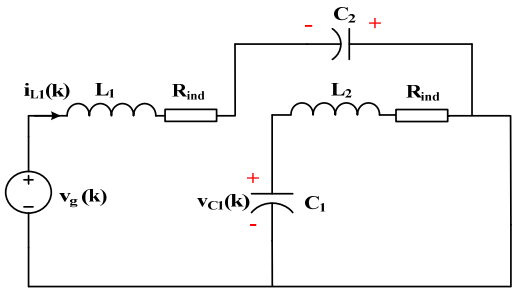

(b) Shoot-through case.

Fig. 2. Equivalent circuits of a qZSI.

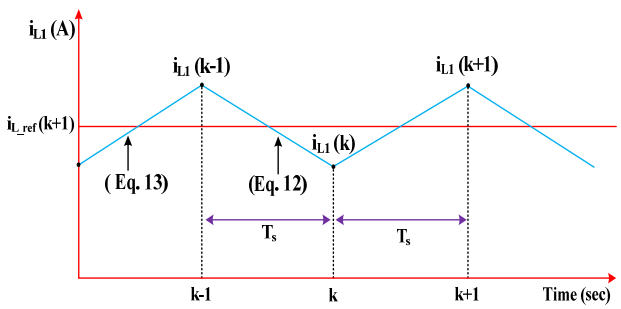

Fig. 3. Waveform of the estimated inductor current.

From the aforementioned analysis, the inductor current is a key factor in the prediction behavior of the capacitor voltage in future. Therefore, its value should be specified. All the previous MPC algorithms for a qZSI [18]-[23], [25] require a current sensor for the inductor current. In this paper, the inductor current is predicted.

The required information to obtain the inductor current value is via storing the previous applied state on the inverter switches (this state gave the minimum cost function). Then, the inductor current is estimated according to the previous state (x_{old}), the capacitor voltage at this state $v_{C_1}(k-1)$ and the previous inductor current $i_{L_1}(k-1)$ as follows:

If (x_{old}) in the non shoot-through case:

$$i_{L_1}(k) = \frac{T_s.(v_g(k)-v_{C_1}(k-1))+L_1.i_{L_1}(k-1)}{L_1+R_{ind}.T_s} \quad (12)$$

If (x_{old}) in the shoot-through case:

$$i_{L_1}(k) = \frac{T_s.v_{C_1}(k-1)+L_1.i_{L_1}(k-1)}{L_1+R_{ind}.T_s} \quad (13)$$

Fig. 3 shows the proposed estimation for inductor current. However, this estimation should be validated versus the common algorithm with current sensors.

TABLE I

COMPARISON OF THREE ALGORITHMS IN TERMS OF COMPUTATIONAL POWER

Eq.	3	6	7	10	11	12	13	15	Sum
Proposed Algorithm	8 × 3	1 × 3	7 × 3	1 × 3	1 × 3	1 × 3		8 × 3	81
Algorithm in [23]	7 × 2	1 × 3	7 × 2	1 × 3	0	-	-	7 × 2	48
Algorithm in [21]	8 × 3	7 × 3	7 × 3	1 × 3	1 × 3	-	-	8× 3	96

The next step is to set the reference values for capacitor voltage and inductor current. According to the required output power, the reference inductor current is calculated as in (14). For the capacitor voltage, it should be at least two times higher than the peak phase voltage [2].

$$i_{L\_ref} = \frac{P_{o\_ref}}{v_g(k)} \quad (14)$$

B. Cost Function Definition

The future values of the controlled variables are calculated during all the converter switching states, except for the inductor current prediction, and compared with the reference values to compose the cost function $g(x)$ as stated in (15). The cost function is computed in every switching state and the state with the minimum cost function is selected to be the next optimized switching state of the converter. For the prediction value of the inductor current in the non shoot-through case, it will only calculated once in each cycle instead of every iteration of the loop where it has the same value [23]. This shortens the execution time of the proposed MFCS-MPC. A flowchart of the proposed control system is shown in Fig. 4. In addition, the cost function is found as:

$$\begin{aligned} g(x) = \lambda_{io} &\left|i_{\alpha_{ref}}(k+1) - i_{\alpha_o}(k+1)\right| \\ &+ \left|i_{\beta_{ref}}(k+1) - i_{\beta_o}(k+1)\right| \\ &+ \lambda_{vc}\left|v_{C_{ref}}(k+1) - v_{C1}(k+1)\right| \\ &+ \lambda_{iL}\left|i_{L\_ref}(k+1) - i_{L1}(k+1)\right| \end{aligned} \quad (15)$$

Table I summarizes the number of iterations for each equation in the three algorithms over three cascaded sampling periods. In the proposed algorithm, the inductor current sensor is removed and its value is estimated. This adds only 3 iterations. On other hand, the number of iterations for (6) decreases to only 3 iterations when compared to [21]. It is worth noting that however the proposed algorithm has more iterations than the proposed one in [23], it has the advantage of removing the current sensor.

III. SIMULATION RESULTS

Simulations have been executed on a qZSI with the parameters listed in Table II based on MATLAB/SIMULINK.

TABLE II
SIMULATION AND EXPERIMENTAL PARAMETERS

Parameter	Symbol	Value
Input voltage	v_g	70 V
qZS inductance	$L_1 = L_2$	6 mH
qZS capacitance	$C_1 = C_2$	470 µF
Inductor Resistance	R_{ind}	400 mΩ
Resistance of the load	R	12 Ω /phase
Inductance of the load	L	24.5 mH/ phase
Sampling time	T_s	75 µsec
Line Frequency	f	50 Hz

MATLAB solver is adjusted to execute the program at a fixed-step size with sampling time of 1µsec and a single-tasking mode. Two steps should be done to validate the proposed model. The first one is to compare the results of the proposed sensorless MFCS-MPC with a common FCS-MPC with sensor to confirm that the current observer is working fine. The simulation results of the estimated inductor current compared to the actual current under MFCS-MPC are depicted in Fig. 5. The two currents are identical which confirms the proposed idea. The second step is to apply an assessment of the proposed MFCS-MPC with a current observer for a qZSI versus the traditional PID controller under the same power circuit, reference values, averaging switching frequency, and sampling period.

To carify the comparison, the control parameters of the linear PID are described first. Based on the small signal analysis of a qZSI in [2], the transfer function that combines the capacitor voltage $v_{C_1}(k)$ and the shoot-through duty ratio (d_o) is:

$$G(s) = \frac{\hat{v}_{c1}(s)}{\hat{d}_o(s)} = \frac{(V_{C_1}+V_{C_2}-R_{ind}.I_{Load})(1-2D_o)+(I_{Load}-I_{L_1}-I_{L_2})(L.s+R_{ind})}{L_1.C_1.s^2+C_1.R_{ind}.s+(1-2.D_o)^2} \quad (16)$$

From the above transfer function, it can be seen that there is a right-half-plane (RHP) zero in the boosting mode. Then the control system has a non-minimum phase phenomena. Thus, the control design development is challenging. Based on the SISO tool in MATLAB, the PID compensator has been designed to obtain a good phase margin (60°) and crossover frequency (628 rad/sec), and its equation is presented in (17). The frequency response for the closed-loop gain system is depicted in Fig. 6. PID linear control has stabilized the qZSI with a phase margin of 60 degrees.

$$G_c(s) = \frac{0.1342(0.007s+1)(0.022s+1)}{s(0.00018s+1)} \quad (17)$$

Regulating the capacitor voltage means adjusting the DC side. The output of the compensator directly gives the shoot-through duty cycle that retains the capacitor voltage at its reference value. After that, the AC current is controlled using the current regulator.

After a brief description of PID control, different tests will

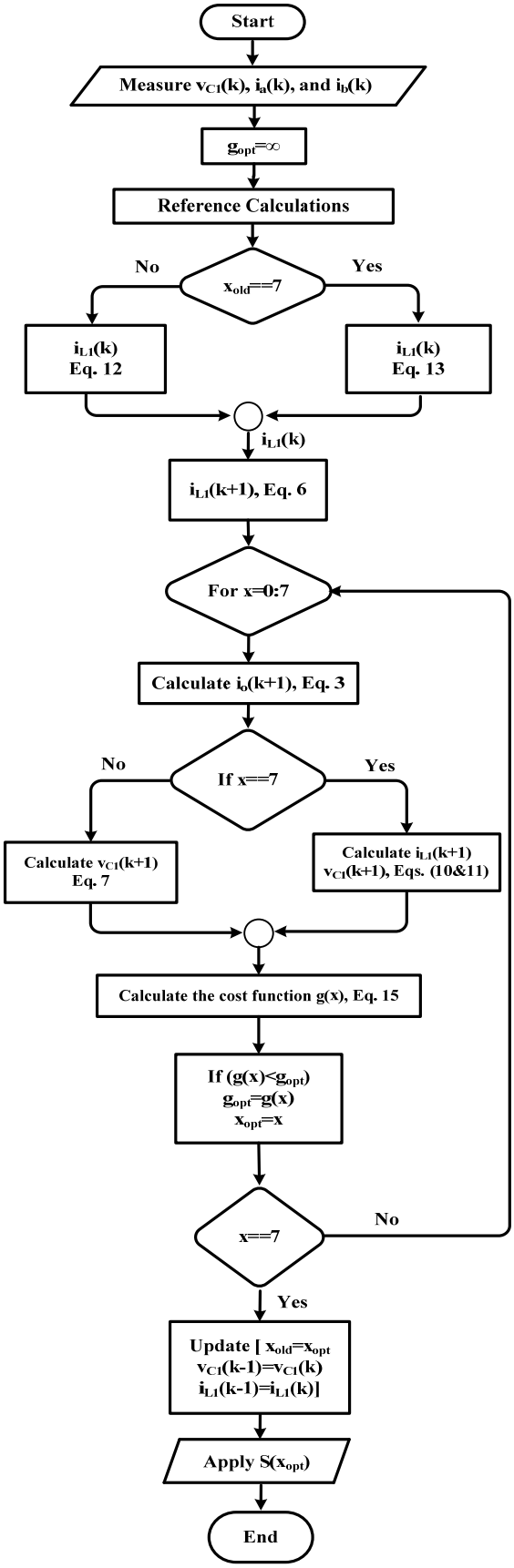

Fig. 4. Proposed MFCS-MPC algorithm for a qZSI.

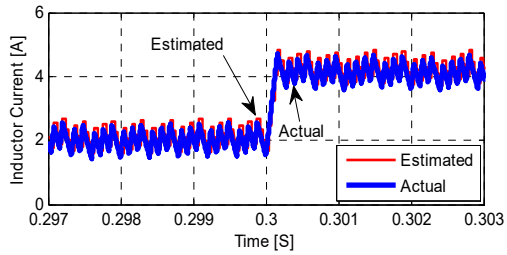

Fig. 5. Estimated inductor (L_1) current generated from the proposed control block and actual inductor current.

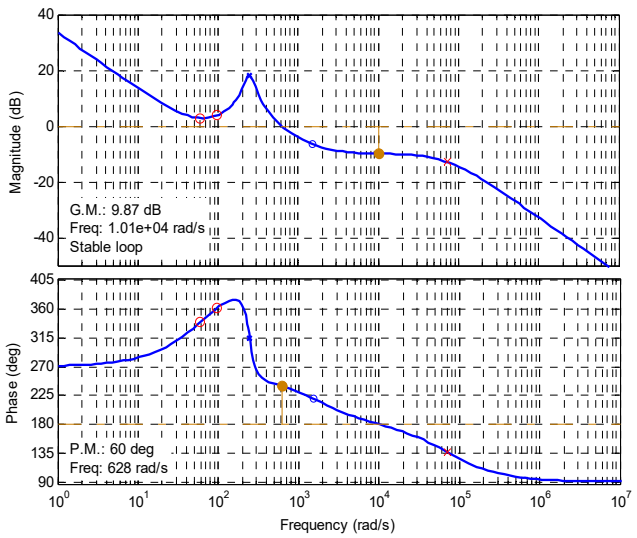

Fig. 6. Bode plot of the closed loop transfer function with a PID controller.

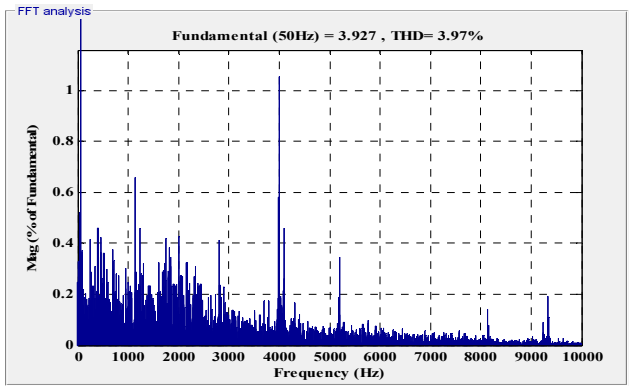

(a) MFCS-MPC.

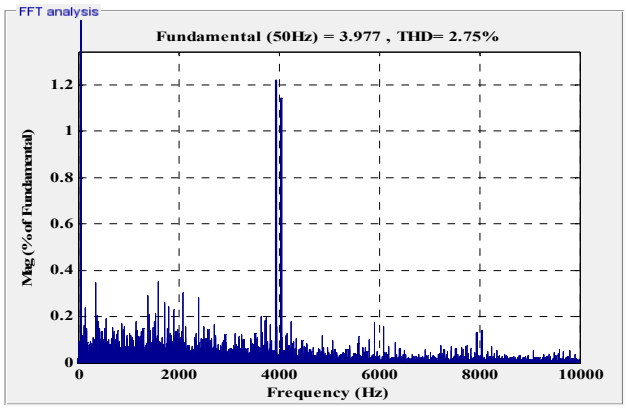

(b) PID controller.

Fig. 7. FFT spectrum for load current.

be applied for both the MFCS-MPC with a current observer for a qZSI versus a traditional PID controller. The reference power of the load is stepped up from 150 W to 300 W at 0.3 sec. There is an inherent relation among the modulation index (M) and the shoot-through duty cycle (D) where operating at a large (M) leads to a small (D). Thus, a low boosting factor is achieved. To avoid this conflict, the capacitor reference voltage for the qZSI is established to be larger than twice the peak phase voltage. Here, the peak phase voltage is achieved at the maximum operating output power due to the constant impedance of the RL load. Thus, the set point of the capacitor voltage is equal to 120 V.

In fact, FCS-MPC gives a variable switching frequency from one operating point to another. The switching state of the inverter can be changed only once during each sampling instant. Thus, the maximum possible switching frequency is limited by half of the sampling frequency [27]. However, the switching states do not change at every sampling instant. Therefore, the average switching frequency is always less than half the sampling frequency. Additionally, the switching frequency in FCS-MPC can be controlled by adding it as an extra term in the cost function. Consequently, to make a justified assessment between the two controllers, they have to operate at the same average switching frequency.

The average value for the MFCS-MPC is obtained from a FFT analysis of the load current at an output power of 300 W. The harmonics spectrum is centered at 4 kHz as shown in Fig. 7(a). In the PWM scheme, the shoot-through is executed twice per switching period. Therefore, the frequency of PWM carrier is chosen to be 2 kHz [27]. Moreover, the FFT analysis of the load current with a PID controller is shown in Fig. 7(b). From the previous discussion, the switching frequency of the system is low. To avoid operating the converter in the Discontinuous Conduction Mode (DCM), the two inductors of a qZS network have a large value of the inductance (6 mH). The values of the weighting factors λ_{io}, λ_{vc} and λ_{iL} are set as 0.3, 0.33 and 1, respectively, for the FCS-MPC control. Finally, a discrete PID block in MATLAB/SIMULINK is used to implement the current control mode of the AC side with the proportional gain at 10 and the integral gain at 30. The modified simple boost control technique [28] is used to generate the shoot-through duty cycle due to its simplicity at the implementation of the experimental work.

A very important factor for measuring the quality of any control strategy is the dynamic response of the controlled variables in tracking their set-points under a load step change. For a qZSI, the dynamic behavior of the capacitor voltage and the load current are the main comparative factors. The power is stepped from 150 W to 300 W for both the MFCS-MPC and PID controllers. Figure 8 shows the response of the three-phase load currents under this change (lower part) for the three

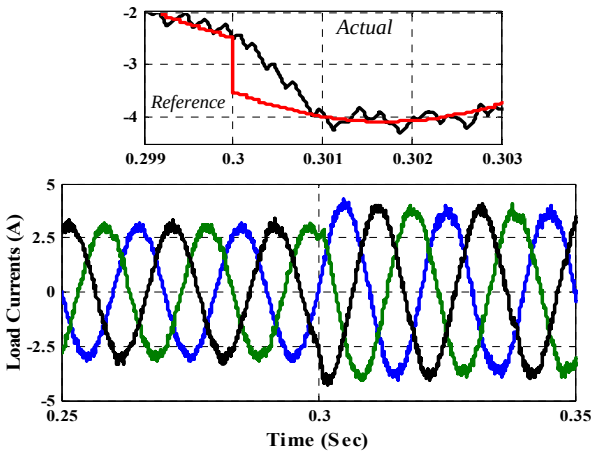

(a) MFCS-MPC.

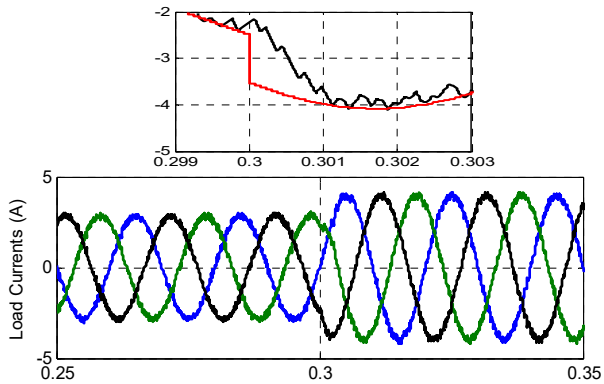

(b) FCS-MPC.

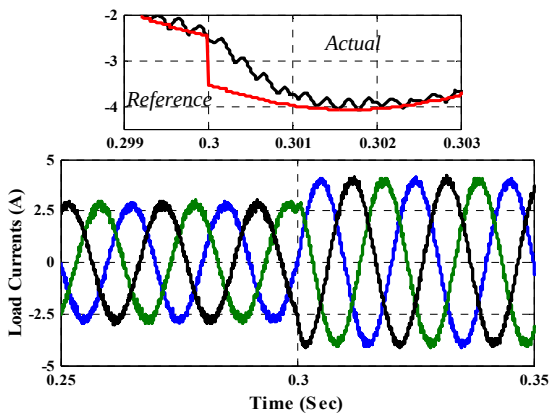

(c) PID controller.

Fig. 8. Load current response under a power reference step from 150 W to 300 W. (Lower figure: Three-phase load currents. Upper figure: Zoomed view of phase (a) and its reference).

different controls.

It is worth noting that the output voltage is not constant (a RL load with the current control mode). Therefore, for a power change from 150 W to 300 W, the peak load current changes from 2.88 A to 4.02 A. Then a zoomed view of the reference signal of the phase current and the actual phase current are shown in the upper part of the figure. It is clear that the generated value for the load current tracks the reference one and reaches steady-state within 1 msec for the

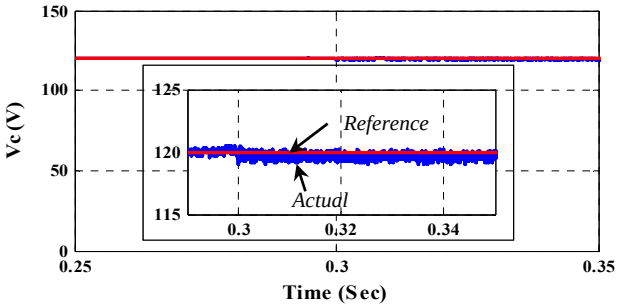

(a) MFCS-MPC.

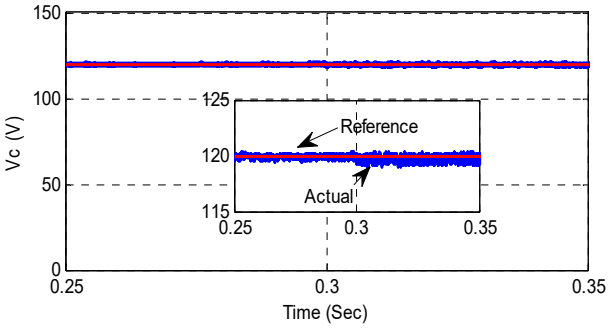

(b) FCS-MPC.

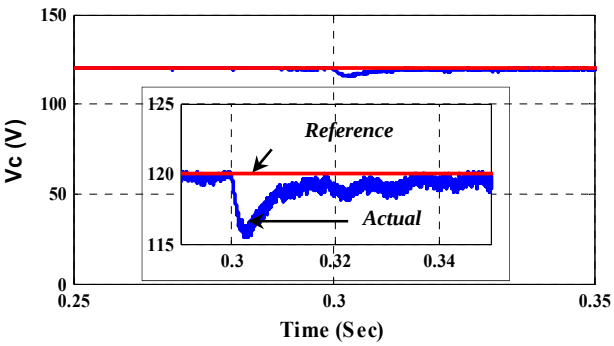

(c) PID controller.

Fig. 9. Capacitor voltage response under a power reference change from 150 W to 300 W.

proposed MFCS-MPC, 1 msec sec for FCS-MPC and 1.5 msec for the PID control. This demonstrates the fast response of both MPC techniques over the PID control. Then the dynamic responses of the capacitor voltage with the MFCS-MPC and FCS-MPC techniques are shown in Fig. 9(a) and (b), repectively. However, the PID control is shown in Fig. 9(c) under a step change in the power reference at 0.3 sec. From the three figures, it can be seen that the FCS-MPC techniques remove the undershoot in the capacitor voltage due to the non-minimum phase (capacitor voltage dips before it rises in response of proposed control technique) for a qZSI and force the capacitor voltage to track the reference with very small percent of dipping when compared to the PID.

The simulation results for the inductor (L_1) current with the FCS-MPC techniques and the PID controller are shown in Fig. 10(a), (b) and (c), respectively. The value of average inductor current changes from 2.2 A to 4.3 A. Figure 10(c) shows a noticeably slower dynamic response of the inductor current to

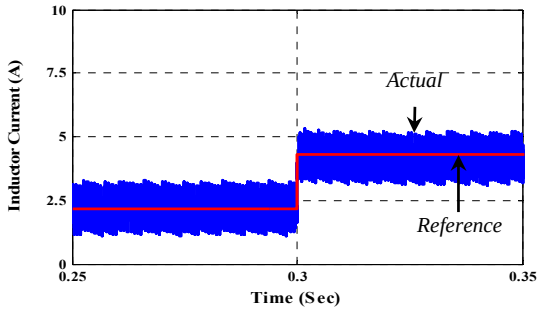

(a) MFCS-MPC.

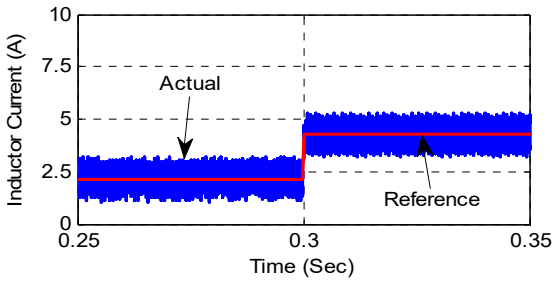

(b) FCS-MPC.

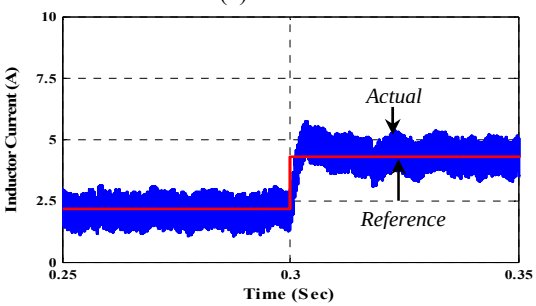

(c) PID controller.

Fig. 10. Inductor (L_1) current under a reference step change.

track its reference point with the PID controller when compared to the proposed MFCS-MPC.

IV. Z-NETWORK CURRENT ESTIMATOR PARAMETER UNCERTAINTY

To demonstrate the effectiveness of the proposed estimation in terms of uncertainty, the values of Z-network inductors and capacitors have been decreased by 10% (as tolerance). Then the system has been examined in simulation

Fig. 11(a) shows the actual and estimator currents with inductor uncertainty (10%) under a load power change from 150 W to 300 W at 0.3 sec. There is no difference between the estimated and actual currents before or after the load power change at applying the inductor uncertainty.

In addition, the capacitor values in the Z-network are decreased by 10% to examine the capacitor uncertainty. Fig. 11(b) shows the actual and estimator currents with capacitance uncertainty (10%) under a change in load power from 150 W to 300 W at 0.3 sec. Again, there is no difference between estimated and actual currents before or after the load power change at applying the capacitor uncertainty.

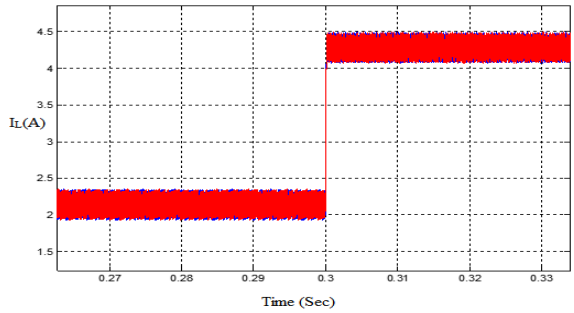

(a) Inductance uncertainty (from 6 to 5.4mH).

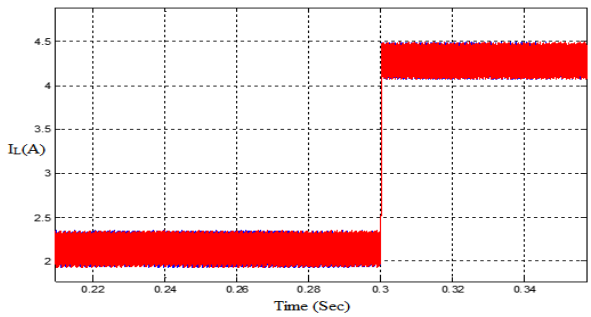

(b) Capacitance uncertainty (from 470 to 423µF).

Fig. 11. Estimator and actual currents under a load power change.

To understand this by looking into (6), the value of the inductor L does not affect the value of the estimation. From (6), $(R_{ind}(k).T_s)$ is very small relative to L_1. In addition, $T_s.(v_g(k) - v_{C_1}(k))$ is very small relative to $L_1.i_{L_1}(k)$. Then by neglecting them, the change effect of L_1 (nominator) cancels L_1 (dominator) and acts independent of L. Note that the uncertainty of the capacitance results in a small change in the capacitor voltage as explained in (7). However, this effects on $v_{C_1}(k)$, which is explained above, as a very small value relative to $L_1.i_{L_1}(k)$. Then it makes the estimator current works independent of both L and C.

V. EXPERIMENTAL RESULTS

A three-phase qZSI prototype has been built in the laboratory as shown in Fig. 12. The same parameters in Table II are used during the experimental test. The digital platform for the experimental work was a TI floating-point digital signal processor DSP TMS320F28335. The Embedded Coder feature in MATLAB/SIMULINK was used to program the digital board for simplifying the implementation of the control system. The available inductor in the test environment is 1.5 mH. Therefore, four inductors have been connected in series to obtain the desired inductance of 6 mH. An external hardware board is used to combine the generated pulses by the DC side controller and AC controller by using a logical (OR) circuit. After that, the resulting signals are inverted before they are applied to the switched devices of the qZSI. The three-phase inverter module is a PM50CLA120 IGBT power module with its integrated gate driver. Results have

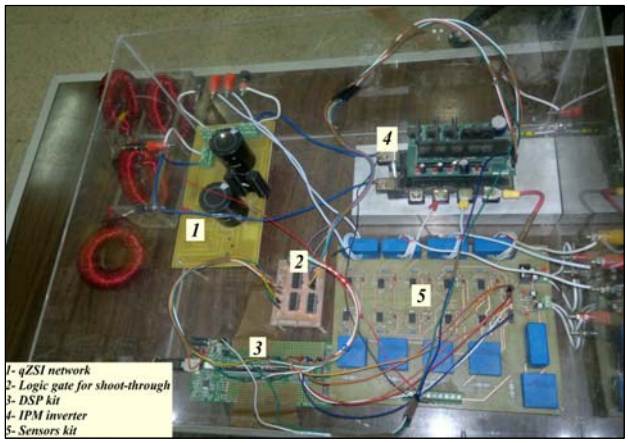

Fig. 12. Experimental setup for the qZSI topology.

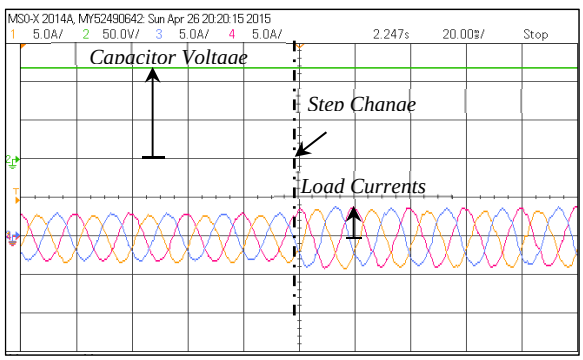

(a) MFCS-MPC.

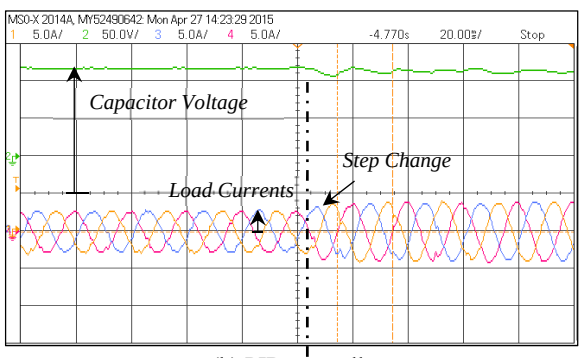

(b) PID controller.

Fig. 13. Experimental results for capacitor voltage (C_1) and three-phase currents under a reference power step-up change.

been obtained for the proposed MFCS-MPC with a current observer and for the PID linear control. The waveforms for the capacitor voltage and load current during a step change of the required output power are shown in Fig. 13(a) for the FCS-MPC and in (b) for the PID controller. It can be observed that during the step change instant, the controlled capacitor voltage of the FCS-MPC shows a good regulation without a noticeable variation from its reference voltage (120 V). On the other hand, the controlled capacitor voltage of the PID compensator has an undershot and a transient oscillation at the instant of power change.

Furthermore, the steady-state experimental results for the capacitor voltage and three-phase load currents at the output

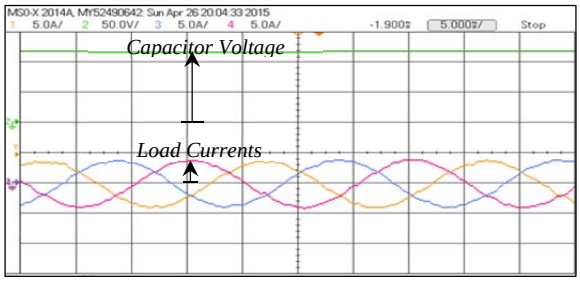

(a) MFCS-MPC controller.

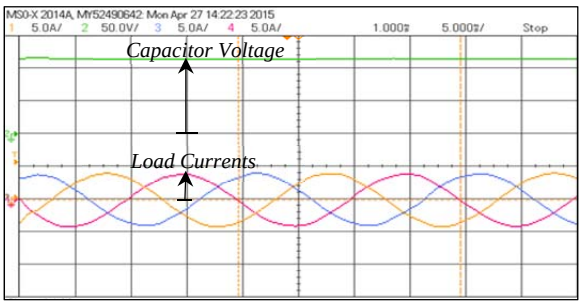

(b) PID controller.

Fig. 14. Experimental results for the capacitor voltage (C_1) and three-phase current at the steady-state.

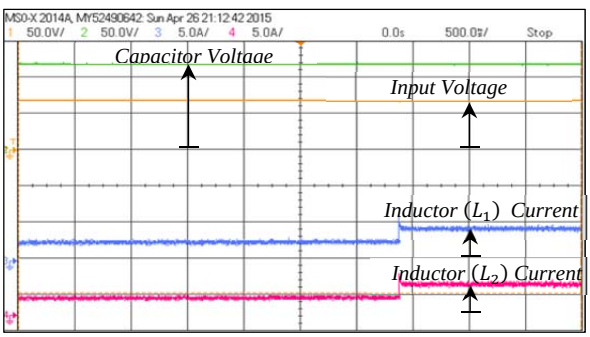

(a) MFCS-MPC.

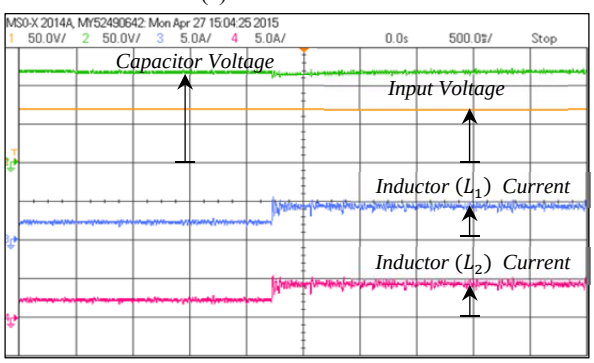

(b) PID controller.

Fig. 15. Experimental results for the DC side under a power reference change from 150 W to 300 W.

power of 300 W are given in Fig. 14(a) and (b) for both the MFCS-MPC and the PID, respectively. It is clear that under steady-state operation, both control techniques are similar. Then Fig. 15(a) and (b) show experimental waveforms of the currents of the two inductors and the capacitor voltage under a power reference change from 150 W to 300 W with the MFCS-MPC and PID, respectively. Fig. 14 shows clearly the

similarity in the inductor currents of (L_1) and (L_2) under a power reference step-up which assures the normal operation of the circuit. In addition, the AC ripple current shown in the experimental results is a miss-record because of the accuracy at the line frequency.

On the other hand, the capacitor voltage shows the superior performance of the proposed MFCS-MPC over the PID control for dynamic behavior. The output load current has similar deviations from a uniform sinusoidal wave. The Total Harmonic Distortion (THD) of the output current is measured experimentally by a Multiver 3HN analyzer at the operating point of 300 W. From the experimental results, the $THD_{MFCS-MPC}$ = 4.4% and the THD_{PID} =3.2%. Therefore, the classic controller gives better performance from the harmonics distortion point of view when compared to the MFCS-MPC. This is due to the fact that the PID operates at a constant switching frequency, while the MFCS-MPC operates at a variable range limited by half of the sampling frequency.

VI. Conclusion

Experimental verification of the proposed modified FCS-MPC algorithm based current observer for a qZSI is provided in this paper. With the presented algorithm, the results confirm the validity of using a current observer for the inductor current instead of using a current sensor. This results save the circuit complicity and cost. To verify the capability of the proposed control, it has been assessed by comparing to the FCS-MPC and classic PID controllers. The simulation and the experimental results concluded that the MFCS-MPC has the merit of high performance in tracking the reference values of the control objectives, especially for the capacitor voltage. On the other hand, PID gives slightly lower THD since it operates at a fixed switching frequency.

Acknowledgment

This work is funded in part by the Egyptian Science and Technology Development Funds (STDF), project ID: 15261.

References

[1] Y. P. Siwakoti, F. Z. Peng, F. Blaabjerg, P. C. Loh, and G. E. Town, "Impedance source networks for electric power conversion part I: A topological review," *IEEE Trans. Power Electron.*, Vol. 30, No. 2, pp. 699-716, Feb. 2015.

[2] Y. Li, S. Jiang, J. G. Cintron-Rivera, and F. Z. Peng, "Modeling and control of quasi-Z-source inverter for distributed generation applications," *IEEE Trans. Ind. Electron.*, Vol. 60, No. 4, pp. 1532-1541, Apr. 2013.

[3] K. Deng, J. Zheng, and J. Mei, "Novel switched-inductor quasi-Z-source inverter," *Journal of power Electronics*, Vol. 14, No. 1, pp. 11-21, Jan. 2014.

[4] O. Ellabban, J. V. Mierlo, and P. Lataire, "A DSP-based dual-loop peak DC-link voltage control strategy of the Z-source inverter," *IEEE Trans. Power Electron.*, Vol. 27, No. 9, pp. 4088-4097, Sep. 2012.

[5] X. Ding, Z. Qian, S. Yang, B. Cui, and F. Peng, "A direct peak DC-link boost voltage control strategy in Z-source inverter," in *Proc. IEEE 22nd Applied Power Electronics Conference (APEC)*, pp. 648-653, 2007.

[6] Y. P. Siwakoti, F. Z. Peng, F. Blaabjerge, P. C. Loh, G. E. Town, and S. Yang, "Impedance-source networks for electric power conversion part II: Review of control and modulation techniques," *IEEE Trans. Power Electron.*, Vol. 30, No. 4, pp. 1887-1906, Apr. 2015.

[7] O. Ellabban, J. V. Mierlo, and P. Lataire, "Capacitor voltage control techniques of the z-source inverter: A comparative study," *European Journal (EPE)*, Vol. 21, No. 4, pp. 13-24, Dec. 2011.

[8] S. Yang, X. Ding, F. Zhang, F. Z. Peng, and Z. Qian, "Unified control technique for Z-source inverter," in *Proc. IEEE Power Electronics Specialists Conference (PESC)*, pp. 3236-3242, 2008.

[9] S. Vazquez, J. I. Leon, L. G. Franquelo, J. Rodriguez, H. A. Young, A. Marquez, and P. Zanchetta, "Model predictive control: A review of its applications in power electronics," *IEEE Ind. Electron. Mag.*, Vol. 8, No. 1, pp. 16-31, Mar. 2014.

[10] P. Alkorta, O. Barambones, J. A. Cortajarena, and A. Zubizarrreta, "Efficient multivariable generalized predictive control for sensorless induction motor drives," *IEEE Trans. Ind. Electron.*, Vol. 61, No. 9, pp. 5126-5134, Sep. 2014.

[11] D.K. Choi and K. B. Lee, "Dynamic performance improvement of AC/DC converter using model predictive direct power control with finite control set," *IEEE Trans. Ind. Electron.,* Vol. 62, No. 2, pp. 757-767, Feb. 2015.

[12] J. Bocker, B. Freudenberg, A. and S. Dieckerhoff, "Experimental comparison of model predictive control and cascaded control of the modular multilevel converter," *IEEE Trans. Power Electron.*, Vol. 30, No. 1, pp. 422-430, Jan. 2015.

[13] C. A. Rojas, J. Rodriguez, F. Villarroel, J. R. Espinoza, C. A. Silva, and M. Trincado, "Predictive Torque and Flux Control Without Weighting Factors," *IEEE Transaction on Industrial Electronics*, Vol. 60, No. 2, pp. 681-690, Feb. 2013.

[14] P. Cortés, S. Kouro, B. La Rocca, R. Vargas, J. Rodríguez, J. L. Leon, S. Vazquez, and L.G. Franquelo, "Guidelines for weighting factors design in model predictive control of power converters and drives," in *Proc. IEEE International Conference on Industrial Technology (ICIT)*, pp. 1-7, 2009.

[15] W. Mo, P. C. Loh, and F. Blaabjerg, "Model predictive control for Z-source power converter," in *Proc. 8th IEEE International Conference on Power Electronics and ECCE Asia (ICPE & ECCE)*, pp. 3022-3028, 2011.

[16] W. Mo, P. C. Loh, and F. Blaabjerg, "Model predictive control of Z-source neutral point clamped inverter," in *Proc. Energy Conversion Congress and Exposition (ECCE)*, pp. 3838-3843, 2011.

[17] W. Mo, P. C. Loh, and F. Blaabjerg, "Maximum power point tracking technique implementation of Z-source inverter through finite step model predictive control strategy," in *Proc. IEEE 7th Conference on Industrial Electronics and Applications (ICIEA)*, pp. 1523-1528, 2012.

[18] M. Mosa, O. Ellabban, H. Abu-Rub, A. Kouzou, and J. Rodríguez, "Model predictive control applied for quasi Z-

source inverter," in *Proc. IEEE 28th Applied Power Electronics Conference (APEC)*, pp. 165-169, 2013.
[19] O. Ellabban, M. Mosa, H. Abu-Rub, and J. Rodriguez, "Model predictive control of a grid connected quasi z-source inverter," in *Proc. IEEE International Conference on Industrial Technology (ICIT)*, pp. 1591-1596, 2013.
[20] M. Mosa, H. Abu-Rub, and J. Rodriguez, "High performance predictive control applied to three phase grid connected quasi-Z-source inverter" in *Proc. IEEE 39th Annual Industrial Electronics Society Conference (IECON)*, pp. 5810-5815, 2013.
[21] M. Mosa, G. M. Dousoky, and H. Abu-Rub, "A novel FPGA implementation of a model predictive controller for SiC-based quasi-Z-source inverters," in *Proc. IEEE 29th Annual Applied Power Electronics Conference (APEC)*, pp. 1293-1298, 2014.
[22] A. Bakeer, M. A. Ismeil, M. Orabi, and R. Kennel, "Control of switched-inductor quasi Z-source inverter (SL-qZSI) based on model predictive control technique (MPC)," in *Proc. IEEE International Conference on Industrial Technology (ICIT)*, pp. 2248-2253, 2015.
[23] A. Bakeer, M. A. Ismeil, and M. Orabi, "A powerful finite control set-model predictive control algorithm for quasi Z-source inverter," *IEEE Trans. Ind. Informat.*, Vol. 12, No. 4, pp. 1371-1379, Aug. 2016.
[24] A. Bakeer, M. A. Ismeil, A. Kouzou, and M. Orabi, "Development of MPC algorithm for quasi Z-source inverter (qZSI)," in *Proc. 3th IEEE International Conference on Control, Engineering & Information Technology (CEIT)*, Algeria, pp. 1-6, 2015.
[25] A. Ayad and R. Kennel, "Direct model predictive control of quasi-Z-source inverter compared with the traditional pi-based PWM control," in *Proc. 17th European Conference on Power Electronics and Applications (EPE/ECCE)*, pp. 1-9, 2015.
[26] C. Xia, M. Wang, Z.Song, and T. Liu, "Robust model predictive current control of three-phase voltage source PWM rectifier with online disturbance observation," *IEEE Trans. Ind. Informat.*, Vol. 8, No. 3, pp. 459-471, Aug., 2012.
[27] J. Rodriguez and P. Cortes, *Predictive Control of Power Converters and Electrical Drives*, John Wiley & Sons, Vol. 40, 1st Edition, Chap. 4, pp. 59, 2012.
[28] X. Ding, Z. Qian, S. Yang, B. Cui, and F. Z. Peng, "A PID control strategy for DC-link boost voltage in Z-source inverter," in *Proc. 22th IEEE Applied Power Electronics Conference (APEC)*, pp. 1145-1148, 2007.

Abualkasim Bakeer was born in Qena, Egypt, in 1990. He received his B.S. and M.S. degrees in Electrical Engineering from the Department of Electrical Engineering, Aswan University, Aswan, Egypt, in 2012 and 2017, respectively. Since 2014, he has been working as a Teaching Assistant in the Department of Electrical Engineering, Faculty of Engineering, Aswan University. His current research interests include power electronics applications such as AC/DC drives and PV generation systems.

Mohamed A. Ismeil received his B.S. and M.S. degrees in Electrical Engineering from South Valley University, Qena, Egypt, in 2002 and 2008, respectively. From October 2010 to January 2013 he was a Ph.D. student in the Department of Electrical Drive Systems and Power Electronics, Technical University of Munich, Munich, Germany, in Channel System Program. He got his Ph.D. degree from Aswan University, Aswan, Egypt, in 2014. Since April 2014, he has been working as an Assistance Professor in the Department of Electrical Engineering, Aswan University. He is a Member of the Aswan Power Electronics Applications Research Center (APEARC), Aswan University. His current research interests include power inverter designs for renewable applications.

Mohamed Orabi received his Ph.D. degree from Kyushu University, Fukuoka, Japan, in 2004. He is presently working as a Professor in the Department of Electrical Engineering, Aswan University, Aswan, Egypt. He is the Founder and Director of the Aswan Power Electronics Application Research Center (APEARC), Aswan University. From June 2011 to July 2014, he was with Enpirion Inc. and Altera Corp. as the Senior Manager of the Altera-Egypt Technology Center. His current research interests include power electronics applications such as switched power supply dc–dc and ac–dc power-factor-correction converters, integrated power management, the modeling and analysis of nonlinear circuits, and power converter design and analysis for renewable energy applications. Dr. Orabi is an Associate Editor of the IET Power Electronics Journal. He received a South Valley University Encouragement Award in 2009, and a National Encouragement Award in 2010 for his great achievements in engineering science.